Segmentation and morphological characterisation of clustered kaolinite clay minerals using deep learning

Theo Örtendahl[1*], *Angela* Casarella[2], and *Jelke* Dijkstra[1]

[1] Department of architecture and civil engineering, Chalmers University of Technology, Gothenburg, Sweden
[2] Department of Civil and Environmental Engineering, Imperial College London, London, UK

1 Introduction

Characterisation of soil fabric at the particle-scale is essential to understand the macroscopic behaviour of soft clay. Soil fabric refers to the 3D organisation, orientation and morphology of clay platelets and the pore volume they enclose [1]. At present, only state-of-the-art imaging techniques such as phase-contrast nano-holo-tomography (nano-CT), provide the submicron length-scale required to image individual clay platelets in their natural saturated state [2].

Despite advances in 3D characterisation, obtaining reliable quantitative descriptors of fabric in clays from nano-CT images remains a challenging task where conventional image processing often falls short. Deep learning computer vision models offer a promising alternative, enabling 3D segmentation of scans of clay without expensive and time-consuming manual tuning. With adequate training data, both general and modality-specific, deep learning-based segmentation models (e.g. Segment Anything Model 2, Mask R-CNN, YOLOv8, 3D U-net) have the potential to resolve the morphology of clay particles at the resolution of the dataset, capturing not only the characteristic anisotropic shape of clay platelets but also the agglomeration of particles in suspensions.

Segmentation of clay particles from tomography data has been approached semantically or in 2D [3, 4] and in 3D for a limited number of particles [5]. However, full 3D segmentation per instance on a large number of clay particles is territory not covered by previous research.

This study investigates clay particle morphology and aggregation in suspension using deep learning-assisted pipelines for segmentation and labelling of 3D images of clay. Because of the scarcity of annotated clay data, the considered deep-learning models were unsupervised, weakly supervised, or pre-trained foundation models. While specialised models, often based on convolutional-neural-network architectures (CNNs) such as U-Net [6], historically outperformed generalist approaches, foundation models trained on large-scale datasets (e.g., SA-1B and SA-V) have recently shown substantial performance gains [7]. In the area of image segmentation, the introduction of vision transformers is seen as pivotal to this development [8]. Even for domain-specific segmentation, models such as MA-SAM [9] and Geo-SAM [10] show increased accuracy compared to nnU-net [11].

In this work, specific results are presented for segmentation performed with the Segment Anything Model 2 (SAM 2, [12]). The distribution of particle orientations of Speswhite kaolin, a monogranular monomineral artificially refined clay, was investigated. The SAM 2-based framework, SAM-IQ (code under development), enables analyses of particle orientation and intra-cluster porosity, providing deeper insight into inter-particle interaction in suspension. Using SAM-IQ, agglomerates (or clusters) of Speswhite kaolin clay particles were unbundled, and the orientations of each individual intra-cluster particles were analysed and compared with that of the broader particle population.

2 Methodology

Speswhite kaolin clay consists of kaolinite minerals, a 1:1 layered silicate mineral with lateral particle dimensions ranging from 100 nm to 4 µm [1]. Its relatively coarse particle size (in comparison to other clay minerals) makes it a suitable model clay for fundamental fabric analysis using currently available advanced imaging techniques. In contrast, natural clay which typically consist of mixed mineral assemblages, contain significant amounts of inter-particle water, which reduces phase contrast and can hinder particle delineation in nano-holo-tomography. Artificially refined kaolin therefore enables higher resolution imaging with clearer pore-particle discrimination.

In this study, Speswhite kaolin clay was suspended in an aqueous solution at pH 4±1 to promote cluster formation that provides further segmentation challenges. The clay concentration of the liquid was 10 g L^{-1} and it was pipetted into a cylindrical quartz capillary tube with an outer diameter of 300 µm and wall thickness of 10 µm. A short resting period followed, where the largest particles were allowed to settle to the bottom, leaving smaller more hydrodynamically stable particles in suspension. The clay was imaged at a resolution of 50 nm resulting in a cylindrical image with a diameter of 125 µm and a height of 108 µm. The nano-CT image used in this study was acquired at the ID16B beamline at the European Synchrotron Radiation Facility (ESRF) in Grenoble, France [13].

A cubic volume of 25×25×25 µm was extracted from the reconstructed 3D volume and segmented and labelled using SAM-IQ following the pre- and postprocessing workflow described in [14]. For identifying objects, a find-maxima

* Corresponding author: theoo@chalmers.se

algorithm from the software ImageJ [15] was used slice-by-slice (x-y plane of the 3D image). Furthermore, six representative particle clusters were identified and isolated from the full volume and segmented using the same method.

The resulting instance-segmented images were analysed using the Software for Practical Analysis of Materials (SPAM, [16]) where the orientation of the major axis of each particle was computed.

3 Results

Figure 1 below displays one segmented 2D slice of a clay particle cluster (a) and one selected particle in 3D from different perspectives (b). This particle is outlined in Fig. 1a.

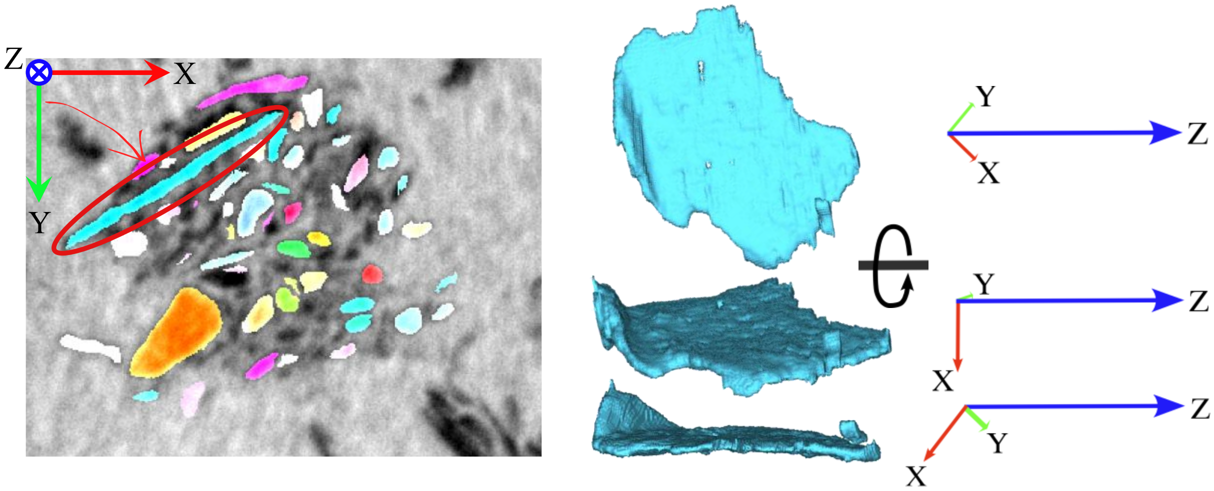

Figure 1. Segmented 2D slice of nano-CT image of Speswhite kaolin clay (a). The coloured overlays represent different clay particles. The blue particle outlined in red is shown in 3D to the right (b) with relative position shown for each rotation in (c).

Whilst not perfect, the SAM-IQ framework identified 916 objects and labelled them for subsequent analyses of descriptors such as particle inclination. The results indicate that there is a preferred orientation of the particles in a suspended kaolin clay sample. Figure 2 demonstrates this in the following Lambert-projection plots, displaying the azimuth and inclination angles for all identified objects. The inclination angles range from 0° (vertical) to 90° (horizontal) and the azimuth covers the entire 360° spectrum.

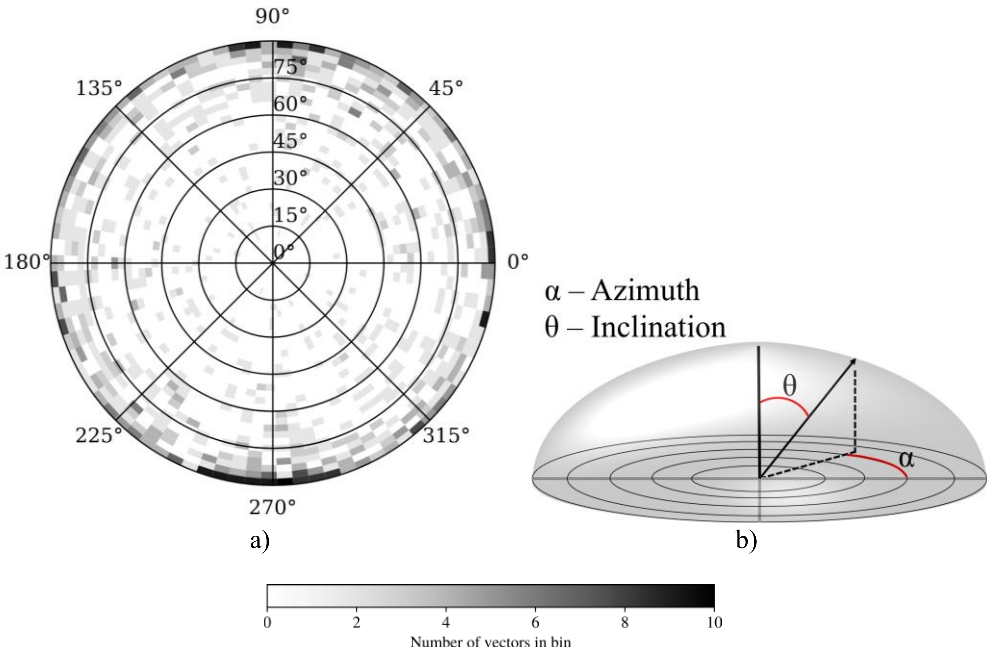

Figure 2. a) Orientation of kaolinite particles using: SAM-IQ and b) visualisation of orientation angles azimuth and inclination.

As is shown in Figure 2, SAM-IQ captures a tendency towards horizontal alignment for the clay particles in suspension. The median inclination of all analysed particles is 83°, where 67% of all particles have an inclination above

75°. When isolating the orientation of particle clusters, however, the results are less distinct with more variation. The median inclination of intra-cluster particles is 53°, where only 20 % of particles have an inclination above 75°. Further, a preferred azimuth angle can be seen for some clusters. This effect is shown below in Figure 3 for four different clusters.

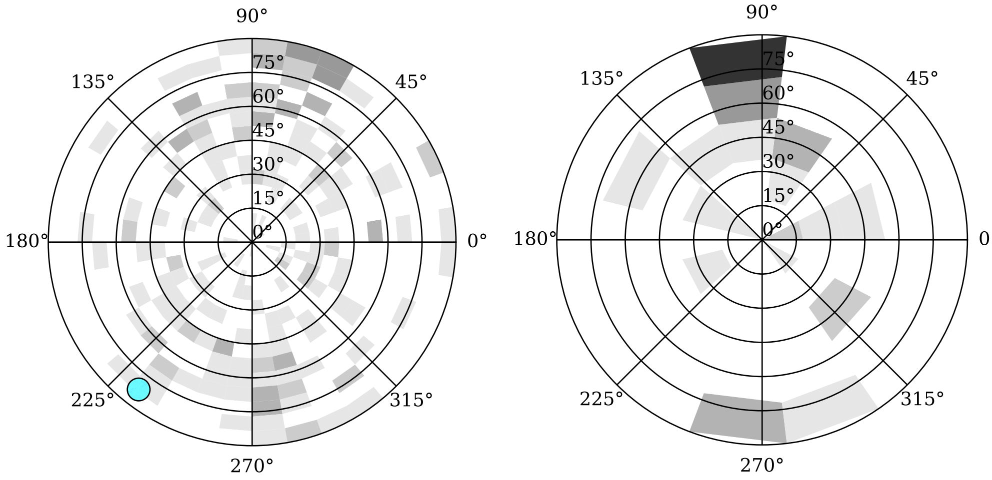

(a) (b)

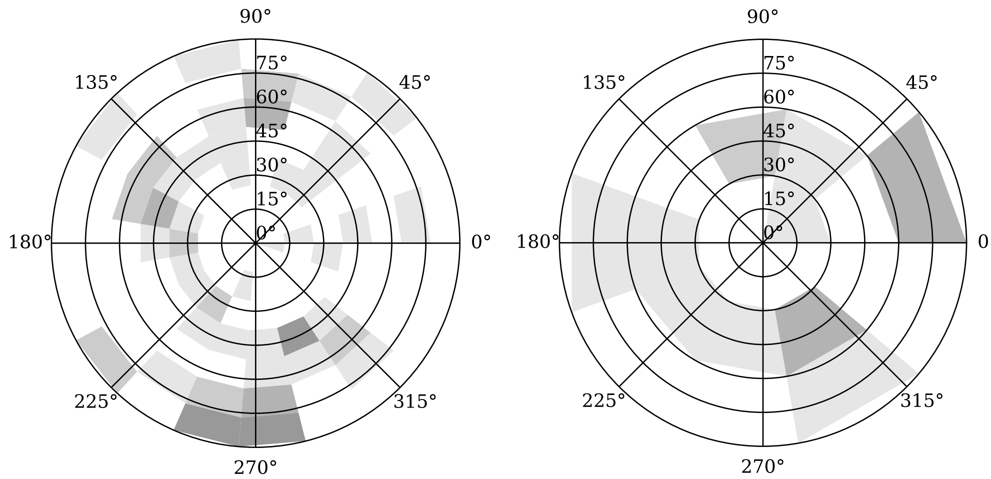

(c) (d)

Figure 3. Orientation of clustered kaolinite particles using SAM-IQ in four separate clusters. (a) shows the orientations of the particles visualised in Fig.1 (a), where the orientation of the particle in Fig.1 (b) is highlighted with a blue dot.

The cluster, whose analysis is shown in Figure 3a, differs from the remaining clusters as it is substantially larger both in volume and number of particles. In cluster a, 217 particles were identified compared to: 32, 67, and 15 in clusters b, c, and d respectively. In Figure 3a, there is a slight preferred azimuth angle around $\alpha = 90°$ and $\alpha = 270°$, as is the case for the much smaller cluster in Figure 3b. In Figure 3c-d, such a pattern is hard to discern, especially so for Figure 3d, possibly due to the small number of particles.

4 Discussion and conclusion

The results demonstrate the potential of deep learning-assisted segmentation for extracting quantitative fabric descriptors from nano-CT images of clay suspensions, such as particle orientation. The SAM-IQ framework enables the identification and labelling of a large number of particles in 3D, making it possible to quantitatively investigate particle-scale organisation in clay systems with little to no training-specific data that would otherwise be extremely difficult to analyse using conventional image-processing approaches.

The particle orientation results indicate that individual clay particles in suspension tend towards horizontal alignment. This behaviour is consistent with the theoretical and experimental expectations for platy particles in viscous fluids [17]. Hydrodynamic forces tend to orient particles such that their largest cross-sectional plane becomes perpendicular to the direction of settling or movement, minimising drag and resulting in preferential horizontal alignment [17].

When considering particles within clusters separately from the entire particle population, the orientation patterns become less pronounced and more variable. This suggests that particle-particle interactions within clusters locally disturb the hydrodynamically favoured alignment. In clustered environments, electrochemical attraction and geometric packing constrains likely influence particle orientation, leading to a more heterogeneous internal fabric.

However, it is important to note that segmentation performance decreases in dense regions, where boundaries are ambiguous or partially unresolved. It should also be mentioned that the sample preparation induced cluster formation due to the slightly lowered pH of the solution. The object-identification step of the workflow especially suffers in these regions, as it is difficult to identify a unique input point for each particle. This limitation may affect the accuracy of some measured descriptors, including particle orientation. On the other hand, orientation is expected to be less sensitive to under- and oversegmentation, since they typically occur among neighbouring particles that share similar orientation. In contrast, metrics such as particle aspect ratio and size are likely to be more strongly affected by segmentation errors.

Nonetheless, the SAM-IQ segmentation framework combined with the ellipsoid-fitting technique for particle metrics extraction enables accurate measurements of clay particles and allows us to study the internal structure of clay particle clusters.

References

1. J.K. Mitchell. The fabric of natural clays and its relation to engineering properties. In. (1956).
2. M. Kampschulte, A.C. Langheinirch, J. Sender, H.D. Litzlbauer, U. Althöhn, J.D. Schwab, et al. Nano-Computed Tomography: Technique and Applications. RoFo Fortschritte auf dem Gebiet der Rontgenstrahlen und der Bildgebenden Verfahren.**188**:146–54;(2016). https://doi.org/10.1055/S-0041-106541, PubMed PMID: 26815120.
3. Z. Chen, X. Liu, J. Yang, E. Little, Y. Zhou. Deep learning-based method for SEM image segmentation in mineral characterization, an example from Duvernay Shale samples in Western Canada Sedimentary Basin. Comput. Geosci.**138**:104450; (2020). https://doi.org/10.1016/J.CAGEO.2020.104450
4. J.K. Chow, Z. Li, Z. Su, Y.H. Wang. Characterization of particle orientation of kaolinite samples using the deep learning-based technique. Acta Geotech.**17**:1097–110;(2022). https://doi.org/10.1007/S11440-021-01266-X/FIGURES/9
5. B. Yu, T.A. Dijkstra, W. Fan, I.J. Smalley, Y.N. Wei, L.S. Deng. Advanced multi-scale characterization of loess microstructure: Integrating µXCT and FIB-SEM for detailed fabric analysis and geotechnical implications. Eng. Geol.**341**:107727;(2024). https://doi.org/10.1016/J.ENGGEO.2024.107727
6. W. Weng, X. Zhu. U-Net: Convolutional Networks for Biomedical Image Segmentation. IEEE Access.;9:16591–603; (2015). https://doi.org/10.1109/ACCESS.2021.3053408
7. D. Ma. Recent advances in deep learning based computer vision. Proceedings - 2022 International Conference on Computers, Information Processing and Advanced Education, CIPAE 2022.174–9;(2022). https://doi.org/10.1109/CIPAE55637.2022.00044
8. M. Musideke, Y. Gao, S. Zhang, K. Feng, A. Abudukelimu, H. Abudukelimu. Review of Application of SAM and Its Improved Models in Image Segmentation. Jisuanji Gongcheng/Comput. Eng.51:16–38;(2025). https://doi.org/10.19678/J.ISSN.1000-3428.0070619
9. C. Chen, J. Miao, D. Wu, Z. Yan, S. Kim, J. Hu, et al. MA-SAM: Modality-agnostic SAM adaptation for 3D medical image segmentation. Med Image Anal.98:103310;(2024). https://doi.org/10.1016/J.MEDIA.2024.103310
10. R.I. Sultan, C. Li, H. Zhu, P. Khanduri, M. Brocanelli, D. Zhu. GeoSAM: Fine-tuning SAM with Multi-Modal Prompts for Mobility Infrastructure Segmentation. [cited 2026];(2023). Available from: https://arxiv.org/abs/2311.11319v4
11. F. Isensee, P.F. Jaeger, S.A.A. Kohl, J. Petersen, K.H. Maier-Hein. nnU-Net: a self-configuring method for deep learning-based biomedical image segmentation. Nature Methods 18:203–11;(2020). https://doi.org/10.1038/s41592-020-01008-z PubMed PMID: 33288961.
12. N. Ravi, V. Gabeur, Y.T. Hu, R. Hu, C. Ryali, T. Ma, et al. SAM 2: Segment Anything in Images and Videos (2024). Available from: https://arxiv.org/abs/2408.00714v1
13. G. Martínez-Criado, J. Villanova, R. Tucoulou, D. Salomon, J.P. Suuronen, S. Labouré, et al. ID16B: a hard X-ray nanoprobe beamline at the ESRF for nano-analysis. J Synchrotron Radiat.23:344–52;(2016). https://doi.org/10.1107/S1600577515019839
14. T. Örtendahl. Deep learning-based methods for segmentation and labelling of clay. (2025). Available from: https://github.com/theoortendahl/SAM-clAI
15. C.T. Rueden, J. Schindelin, M.C. Hiner, B.E. DeZonia, A.E. Walter, E.T. Arena, et al. ImageJ2: ImageJ for the next generation of scientific image data. BMC Bioinformatics.18:1–26;(2017). https://doi.org/10.1186/s12859-017-1934-z PubMed PMID: 29187165.
16. O. Stamati, E. Andò, E. Roubin, R. Cailletaud, M. Wiebicke, G. Pinzón, et al. spam: Software for Practical Analysis of Materials. J Open Source Softw.5:2286;(2020). https://doi.org/10.21105/joss.02286
17. J. Happel, H. Brenner. Low Reynolds number hydrodynamics Mech. of Fluids and Transp. Proc.1;(1983). https://doi.org/10.1007/978-94-009-8352-6